Biogeosciences, 13, 4237–4251, 2016
www.biogeosciences.net/13/4237/2016/
doi:10.5194/bg-13-4237-2016

Evaluation of 4 years of continuous $\delta^{13}C(CO_2)$ data using a moving Keeling plot method

Sanam Noreen Vardag, Samuel Hammer, and Ingeborg Levin

Department of Physics and Astronomy, Institut für Umweltphysik, Heidelberg University, Heidelberg, Germany

Correspondence to: Sanam Noreen Vardag (svardag@iup.uni-heidelberg.de)

Received: 15 March 2016 – Published in Biogeosciences Discuss.: 16 March 2016
Revised: 8 July 2016 – Accepted: 8 July 2016 – Published: 26 July 2016

Abstract. Different carbon dioxide (CO_2) emitters can be distinguished by their carbon isotope ratios. Therefore measurements of atmospheric $\delta^{13}C(CO_2)$ and CO_2 concentration contain information on the CO_2 source mix in the catchment area of an atmospheric measurement site. This information may be illustratively presented as the mean isotopic source signature. Recently an increasing number of continuous measurements of $\delta^{13}C(CO_2)$ and CO_2 have become available, opening the door to the quantification of CO_2 shares from different sources at high temporal resolution. Here, we present a method to compute the CO_2 source signature (δ_S) continuously and evaluate our result using model data from the Stochastic Time-Inverted Lagrangian Transport model. Only when we restrict the analysis to situations which fulfill the basic assumptions of the Keeling plot method does our approach provide correct results with minimal biases in δ_S. On average, this bias is 0.2 ‰ with an interquartile range of about 1.2 ‰ for hourly model data. As a consequence of applying the required strict filter criteria, 85 % of the data points – mainly daytime values – need to be discarded. Applying the method to a 4-year dataset of CO_2 and $\delta^{13}C(CO_2)$ measured in Heidelberg, Germany, yields a distinct seasonal cycle of δ_S. Disentangling this seasonal source signature into shares of source components is, however, only possible if the isotopic end members of these sources – i.e., the biosphere, δ_{bio}, and the fuel mix, δ_F – are known. From the mean source signature record in 2012, δ_{bio} could be reliably estimated only for summer to (-25.0 ± 1.0) ‰ and δ_F only for winter to (-32.5 ± 2.5) ‰. As the isotopic end members δ_{bio} and δ_F were shown to change over the season, no year-round estimation of the fossil fuel or biosphere share is possible from the measured mean source signature record without additional information from emission inventories or other tracer measurements.

1 Introduction

A profound understanding of the carbon cycle requires closing the atmospheric CO_2 budget at a regional and global scale. For this purpose it is necessary to distinguish between CO_2 contributions from oceanic, biospheric and anthropogenic sources and sinks. Monitoring these CO_2 contributions separately is desirable to improve process understanding, to investigate climatic feedbacks on the carbon cycle and also to verify emission reductions and design CO_2 mitigation strategies (Marland et al., 2003; Gurney et al., 2009; Ballantyne et al., 2010).

A possibility to distinguish between different CO_2 sources and sinks utilizes concurrent $^{12}CO_2$ and $^{13}CO_2$ observations in the atmosphere. The carbon isotope ratio can be used to identify and even quantify different CO_2 emitters if every emitter has its specific known $\delta^{13}CO_2$ signature. For example, the CO_2 fluxes from land and ocean can be distinguished using the ratio of stable carbon isotopologue $^{13}CO_2$/$^{12}CO_2$ in addition to CO_2 concentration measurements (Mook et al., 1983; Ciais et al., 1995; Alden et al., 2010). In other studies, measurements of $^{13}CO_2$ have been used to distinguish between different fuel types (Pataki, 2003; Lopez et al. 2013; Newman et al., 2016) or to evaluate ecosystem behavior (Torn et al., 2011), to mention but a few examples of the many published in the literature.

In the last decade, new optical instrumentation has been developed, simplifying continuous isotopologue measure-

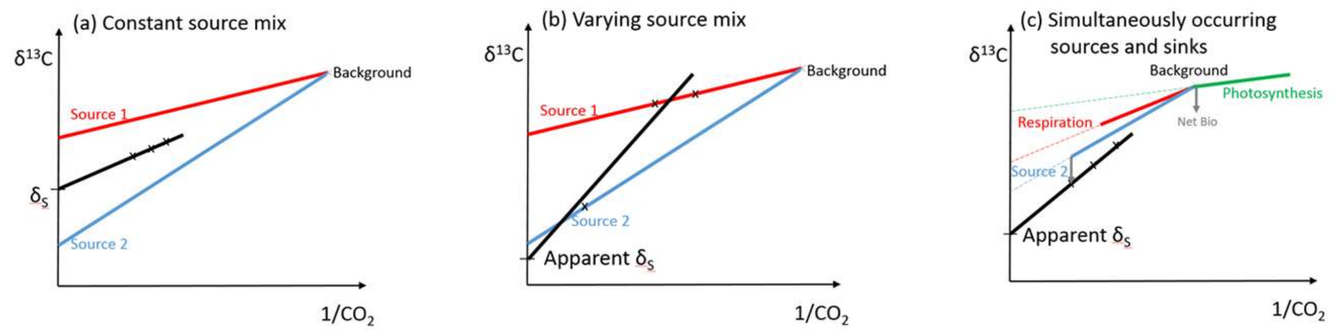

Figure 1. Regression-based determination of source signature using a Keeling plot. For clarity of illustration, we only draw three data points instead of five, which we use for our computation. **(a)** Constant source mix during the time of source signature determination leads to the correct flux-weighted mean isotopic signature (following Eq. A1), δ_S. **(b)** Change of source mix during the period of determination of a Keeling plot due to either a temporal change of emission characteristics or a wind direction change (transportation) leads to a biased result. These situations can be usually identified by a large error of the intercept, δ_S (we choose an error > 2 ‰ to reject these results). **(c)** Sources and sinks with different isotopic signatures or sink fractionation occur at the same time and lead to a wrong apparent source signature. Strong biases are prevented by choosing a minimum net CO_2 concentration range of 5 ppm and demanding a monotonous increase of CO_2 during the 5 h (see text for more details). Note that the background value is displayed for illustration, but it is not used in the moving Keeling plot method.

ments. This has led to an increasing deployment of these instruments, thereby increasing the temporal and spatial resolution of $^{13}C(CO_2)$ and CO_2 data (Bowling et al., 2003; Tuzson et al., 2008; McManus et al., 2010; Griffith et al., 2012; Vogel et al., 2013; Vardag et al., 2015a; Eyer et al., 2016). These data records may lead to an improved understanding of regional CO_2 fluxes, allowing estimates of mean $\delta^{13}C$ source signatures at high temporal resolution. Estimating mean source signatures from concurrent $\delta^{13}C(CO_2)$ and CO_2 records over time provides, e.g., insight into temporal changes in the signatures of two different CO_2 sources such as fossil fuels and the biosphere if their relative share to the CO_2 offset is known. This may be used to study biospheric responses to climatic variations like drought, heat, floods, vapor pressure deficit etc. (Ballantyne et al., 2010; 2011; Bastos et al., 2016). Likewise, the mean source signature can be used to separate between different source CO_2 contributions if the isotopic end members of these sources are known at all times (Pataki, 2003; Torn et al., 2011; Lopez et al. 2013; Moore and Jacobson, 2015; Newman et al., 2016).

Many studies have successfully used the Keeling or Miller–Tans plot method (Keeling, 1958; 1961; Miller and Tans, 2003) to determine source signatures in specific settings (e.g., Pataki, 2003; Ogée et al., 2004; Lai et al., 2004; Knohl et al., 2005; Karlsson et al., 2007; Ballantyne et al., 2010). However, the situations in which Keeling and Miller–Tans plots yield correct results need to be selected carefully (Miller and Tans, 2003). Only if all possible pitfalls are precluded can the Keeling intercept (or the Miller–Tans slope) be interpreted as the gross flux-weighted mean isotopic signature of all CO_2 sources and sinks in the catchment area of the measurement site. Especially in polluted areas with variable source–sink distribution, estimation of isotopic signature using a Keeling or Miller–Tans plot requires a solid procedure, e.g., accounting for wind direction changes or simultaneously occurring CO_2 sinks and sources.

In this study, we discuss the possible pitfalls of CO_2 source signature determination from a continuous dataset using the Keeling plot method and follow a specific modification of this method for automatic retrieval of mean source signature with minimal biases. We test this method with model-simulated CO_2 mole fraction and $\delta^{13}C(CO_2)$ data. Using a modeled dataset where all source signatures are known enables us to test if the calculated source signature is correct, which is vital when evaluating measured data with an automated routine. Having found a method to determine the isotopic signature of the mean source correctly from measured CO_2 and $\delta^{13}C(CO_2)$ data, we discuss which information can be reliably extracted from these results.

2 Methods

2.1 Keeling and Miller–Tans plot method

Keeling (1958, 1961) showed that the mean isotopic signature of a source mix can be calculated by re-arranging the mass balance of total CO_2,

$$CO_{2\mathrm{tot}} = CO_{2\mathrm{bg}} + CO_{2\mathrm{S}}, \tag{1}$$

and of $\delta^{13}C$ of total CO_2, i.e., δ_{tot},

$$\delta_{\mathrm{tot}} \cdot CO_{2\mathrm{tot}} = \delta_{\mathrm{bg}} \cdot CO_{2\mathrm{bg}} + \delta_{\mathrm{S}} \cdot CO_{2\mathrm{S}} \tag{2}$$

to

$$\delta_{\mathrm{tot}} = CO_{2\mathrm{bg}}/CO_{2\mathrm{tot}} \cdot (\delta_{\mathrm{bg}} - \delta_{\mathrm{S}}) + \delta_{\mathrm{S}}, \tag{3}$$

where CO_{2bg} and δ_{bg} are the concentration and $\delta^{13}C(CO_2)$ of the background component and CO_{2S} and δ_S are the concentration and $\delta^{13}C(CO_2)$ of the mean source, respectively. Plotting δ_{tot} vs. $1 / CO_{2tot}$ yields a y intercept of δ_S (cf. Fig. 1a).

Miller and Tans (2003) have suggested an alternative approach to determine the mean isotopic signature by rearranging Eqs. (1) and (2) such that δ_S is the regression slope when plotting $CO_{2tot} \cdot \delta_{tot}$ vs. CO_{2tot}:

$$CO_{2tot} \cdot \delta_{tot} = \delta_S \cdot CO_{2tot} - CO_{2bg}(\delta_{bg} - \delta_S). \quad (4)$$

They argue that this approach might be advantageous since the isotopic signature does not need to be determined from extrapolation to $1 / CO_2 = 0$, which could introduce large errors in the δ_S estimate. Zobitz et al. (2006) have compared the Keeling and the Miller–Tans plot method (Eqs. 3 and 4) and found no significant differences between both approaches when applied to typical ambient CO_2 variations. We were able to reproduce this result with our model-simulated dataset (cf. Sect. 3.1). Differences between both approaches were (0.00 ± 0.04) ‰ when applying certain criteria (standard deviation of intercept < 2 ‰, CO_2 range within $5\,h > 5$ ppm), which will be explained in Sect. 2.3. The choice of fitting algorithm has also been discussed in the literature. Pataki (2003), Miller and Tans (2003) and Zobitz et al. (2006) compared different fitting algorithms for the regression and came up with different recommendations. Orthogonal distance regression (ODR) and weighted total least-squares (WTLS) fits (model 2 fits) take into account errors on x and y, whereas ordinary least-squares (OLS) minimization (model 1 fit) only takes into account y errors. Zobitz et al. (2006) have found differences between both fitting algorithms especially at small CO_2 ranges. We have also applied a model 1 (OLS) and model 2 (WTLS) fit to our simulated data and have not found any significant differences ((0.00 ± 0.01) ‰) between them when applying certain criteria (error of intercept < 2 ‰, CO_2 range within $5\,h > 5$ ppm; see Sect. 2.3). In our study, we use a WTLS fit (Krystek and Anton, 2007) as a stable algorithm for fitting a straight line to a dataset with uncertainty in x and y direction in a Keeling plot method. Note that the isotopic signature of the mean source δ_S can be determined from linear regression without requiring a background CO_2 and $\delta^{13}C(CO_2)$ value. However, the Keeling and Miller–Tans plot methods are only valid if the background and the isotopic signature of the source mix δ_S are constant during the period investigated (Keeling, 1958; Miller and Tans, 2003). Further, the approaches are only valid when sources and sinks do not occur simultaneously. Miller and Tans (2003) gave an example which showed that as soon as sources and sinks of different isotopic signature/fractionation occur simultaneously, the determination of isotopic signature of the source–sink mix may introduce biases. In these cases, the results cannot be interpreted as mean flux-weighted source signature anymore. This has very unfortunate consequences, since in principle we are interested in determining the isotopic signature of the source mix of a region during all times, i.e., also during the day, when photosynthesis cannot be neglected.

2.2 Moving Keeling plot method

For a continuous long-term dataset, we suggest an automatic routine to determine the mean isotopic signature of the source mix. It is similar to the moving Keeling plot for CH_4 currently suggested by Röckmann et al. (2016). In our case of CO_2, we also have to take into account the possibility of simultaneously occurring sinks and sources, which is not important in the case of CH_4. Our moving Keeling plot method is a specific case of the classical Keeling plot method (Eq. 3) (Keeling, 1961) as it uses only five hourly-averaged measurement points of CO_2 and $\delta^{13}C(CO_2)$, fitting a regression line through these five data points (cf. Fig. 1a, illustrated only for three data points for clarity of inspection). We choose 5 h as a compromise between number of data points, and thus of robust regression, and of source mix constancy. This compromise also manifests itself in such a manner that a window size of 5 h leads to maximum coverage. No background value is included in the regression. The moving Keeling plot method works such that, e.g., for the determination of the mean source signature at 15:00, we use the hourly CO_2 and $\delta^{13}C(CO_2)$ measurements from 13:00 to 17:00 and fit a regression line. Next, for the determination of the source signature at 16:00, we use the CO_2 and $\delta^{13}C(CO_2)$ measurements from 14:00 to 18:00 and so on. Note that this approach leads to a strong autocorrelation of neighboring source signature values.

2.3 Filter criteria of the moving Keeling plot method

In order to prevent pitfalls in the regression-based determination of mean isotopic signature, we set a few criteria for the moving Keeling plots to "filter" out situations in which a Keeling plot cannot be performed. These filter criteria are also similar in type to the ones introduced by Röckmann et al. (2016). We here explain why these filter criteria are needed for CO_2 and how they are set.

A prerequisite for the Keeling plot is that the source mix and the background need to stay constant during the investigated period (see Fig. 1a). Varying source mixes may occur when, e.g., the wind direction and therewith the footprint of the measurement site change, or if the emission patterns themselves change over time. This may lead to strong biases of the regression-based mean isotopic source signature (illustrated in Fig. 1b). We eliminate these cases by inspecting the error of the determined intercept δ_S. If the source mix or the background significantly change within 5 h, the data points will not fall on a straight line and the error of the intercept will increase. We here set an error of 2 ‰ (in a WTLS fit) as a threshold between an acceptable and a "bad" fit, after having inspected many Keeling plots individually. Also, we demand a monotonous increase of CO_2 within 5 h, as a decrease would be due to either a sink of CO_2 or a breakdown of the boundary layer inversion potentially associated with a change of catchment area of the measurement, both biasing the resulting mean source signature.

As mentioned before, the determination of a mean isotopic signature is not per se possible during the day when CO_2 sinks and sources are likely to occur simultaneously (Miller and Tans, 2003). This can be explained in the Keeling plot by the vector addition of CO_2 source and sink mixing lines with different isotopic signatures, resulting in a vector with an intercept different from the expected one, leading to an isotopic signature which can even lie outside the expected range of the isotopic source end members (see Fig. 1c). This potential bias is stronger the smaller the net CO_2 signal is. Therefore, e.g., for evaluation of the Heidelberg data, we demand an increase in CO_2 during the 5 h period of at least 5 ppm to exclude periods where the photosynthetic sink is similarly strong to total CO_2 sources. This normally leads to an exclusion of daytime periods, when the boundary layer inversion typically breaks up and the photosynthetic sink is most pronounced. Therefore, we are mainly rejecting periods in which isotopic discrimination during photosynthesis dominates the mean isotopic source signature. During winter, it may happen that the inversion does not break up due to the cold surface temperatures, but in this season photosynthetic activity is typically much smaller than fossil fuel emissions, and therefore biases of the regression-based mean source signature are only small.

In the next section, we show that with these filter criteria – i.e., (i) error of the Keeling plot intercept < 2 ‰, (ii) monotonous increase during 5 h and (iii) increase of > 5 ppm during 5 h, which we chose empirically – we are able to successfully reject those source signatures where the underlying assumptions for the Keeling plot method are not met. In Sect. 3.1, we will also briefly discuss how sensitive the result is to the choice of filter criteria. Note that the filter criteria may differ for different measurement sites depending on the source heterogeneity and footprint of the catchment areas. Therefore, respective filter criteria need to be designed individually for each measurement station.

3 Results and discussion

3.1 Evaluation of the moving Keeling plot method

We apply the moving Keeling plot method to a modeled CO_2 and $\delta^{13}C(CO_2)$ dataset. As also pointed out by Röckmann et al. (2016) in their CH_4 study, this has the advantage that we can test and evaluate our filter criteria as we know exactly the individual isotopic source signatures that created the modeled dataset and, thus, the contribution-weighted mean isotopic source signature at every point in time. Details on the Stochastic Time-Inverted Lagrangian Transport (STILT) model (Lin et al., 2003) and on the computation of the modeled CO_2 and $\delta^{13}C(CO_2)$ record as well as of the resulting mean source signature, δ_S^{STILT}, are given in Appendix A.

We apply the same filter criteria to the calculated mean source signature of the STILT-modeled dataset δ_S^{STILT} as to the regression-based mean source signature (Sect. 2.3). The "unfiltered" source signatures (black in Fig. 2a) are 0–2 ‰ more enriched than the "filtered" source signatures (blue). This offset is mainly caused by the daytime source signatures, which are on average more enriched than nighttime source signatures (Fig. 2b) but more likely to be filtered out based on the criteria of Sect. 2.3.

We have now evaluated the moving Keeling plot method and the used filter criteria based on the model data and tested whether they allow a bias-free retrieval of the mean source signature. In Fig. 3a, we compare the regression-based source signatures to the filtered reference source signature of Fig. 2a, which we have extracted from the model. We compare not only the mean difference of the mean source signature but also the hourly differences of the mean source signature as well as the smoothed difference. This enables us to clearly state how well we are able to determine the hourly mean source signature and its long-term trend.

Figure 3a displays the filtered seasonal changes of the source signature exemplary for the year 2012. The moving Keeling plot method is able to extract the seasonal variability of the mean isotopic signature correctly. The median difference (and interquartile range) between the smoothed regression-based (red) and smoothed modeled (blue) approach (both smoothed with 50th-percentile filter with window size of 100 h, no smoothing 50 points in front of large data gaps) is 0.0 ± 0.4 ‰. A smoothing window size of 100 h (ca. 4 days) was chosen, so that synoptical and seasonal variations of δ_S can be seen while diurnal variations are suppressed. On a shorter diurnal timescale, we compare individual hourly results for the source signature (stars in Fig. 3b, c). The interquartile range of the filtered hourly difference between the reference δ_S^{STILT} and the moving Keeling plot signature is about 1.2 ‰ throughout the year, but the median difference is small (0.2 ‰). The source signature of the model reference and moving Keeling plot source signature show the same temporal pattern both in summer and in winter. Further, we find that, if we do not apply all of the criteria described in Sect. 2.3 (unfiltered data in Fig. 3b, c), we see larger differences between regression-based source signature (from the moving Keeling plot) and the STILT reference values.

Note that with the criteria established in Sect. 2.3 we have to reject about 85 % of all estimated source signatures. This seems to be an intrinsic problem for an urban setting with many different sources and sinks. Obviously, in many situations the prerequisites of the Keeling plot method are not fulfilled, and, if not filtered out, these data would introduce biases in the retrieved mean source signature. Depending on the application, it may be worthwhile to loosen the filter criteria to increase the data coverage. For example, if one sets

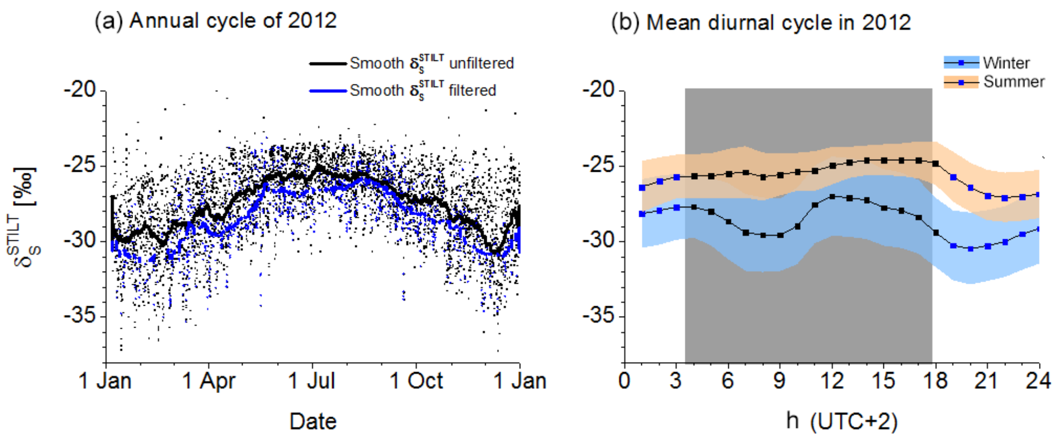

Figure 2. Source signature as calculated with the STILT model following Eq. (A1). **(a)** Unfiltered in black and filtered (for monotonous increase and minimal range) in blue. Only about 15 % of all data points fulfill our strict criteria. However, they are distributed approximately evenly throughout the year. **(b)** Diurnal cycle of modeled mean source signature due to diurnally varying mean source mix. Gray areas denote times when source signature is usually filtered out.

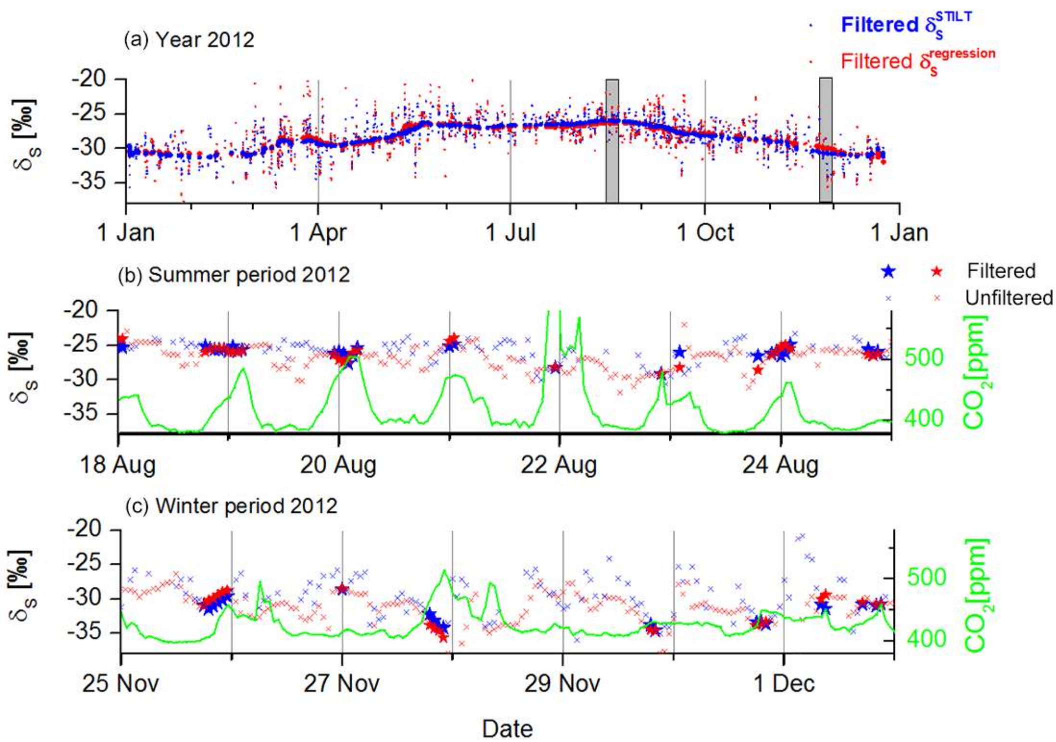

Figure 3. Comparison between modeled reference source signature (blue) and the moving Keeling plot intercept (red), which is regression-based using the modeled CO_2 and $\delta^{13}C(CO_2)$ records. **(a)** Long-term comparison for the year 2012. The smoothed lines of window size 100 are also shown in the respective colors. **(b)** Summer excerpt and **(c)** winter excerpt (gray areas in **a**) of both reference and regression-based source signature. The crosses denote unfiltered data, and bold stars denote filtered data. The green lines in panels **(b)** and **(c)** give the measured CO_2 concentration during the summer and winter periods, respectively.

no criteria for the minimal CO_2 range, but only for the error of the intercept (< 2 ‰), about 60 % of all data remain for the estimated source signature, but the median difference between model- and Keeling-based results increases to 0.3 ‰, and the interquartile range increases to 2.4 ‰ (hourly data), which is about twice what we found before. Withdrawing all filter criteria and using only nighttime values leads to a coverage of about 35 % (nighttime) and an interquartile range of 3.5 ‰. The filter criteria which we use here (Sect. 2.3) are, thus, rather strict, but we are confident to precisely extract the correct source signature from the $\delta^{13}C(CO_2)$ and CO_2 record at the highest temporal resolution.

3.2 The measured source signature record in Heidelberg

We now apply this approach to real measured Heidelberg data. We use the CO_2 and $\delta^{13}C(CO_2)$ record at hourly time resolution (Fig. B1) to compute the isotopic source signature via regression (Fig. 4). The quality of the CO_2 and $\delta^{13}C(CO_2)$ record is assessed in Appendix B. The measurement site and its surrounding catchment area are described by Vogel et al. (2010). We observe a distinct seasonal cycle of the mean isotopic source signature in Heidelberg. Smoothed minimum values of about -32 ‰ are reached in winter. Maximum values of about -26 ‰ occur in summer. This annual pattern is reproduced every year and is similar to annual patterns observed by, e.g., Schmidt (1999) for Schauinsland, Germany, or by Sturm et al. (2006) for Bern, Switzerland. Additionally, the first year shows a more enriched summer maximum source signature. A number of data points (fewer than 0.5 %) lie outside the range of realistic end members between -20 and -45 ‰ of any source in the catchment area (see Table A1). These outliers are not unusual in an urban setting, as the interquartile range of the modeled δ_S for the Heidelberg catchment area is about 1.2 ‰ for hourly (non-smoothed) data, which is only about 30 % higher than the interquartile range of the measured data (see Fig. 4 (1.8 ‰)). The slightly lower variability in the model may be due to a lower variability in the coarse-resolution emission inventory used in STILT ($0.1° \times 0.1°$).

Our 4-year record of the mean source signature in Heidelberg (see Fig. 4) provides a first insight into the source characteristics at the measurement station. It reaches its minimum in winter, when we expect residential heating (mainly isotopically depleted natural gas; see Table A1) to contribute significantly to the source mix. The source signature reaches its maximum in summer, when more enriched biospheric fluxes are expected to dominate the CO_2 signal. This observed seasonal cycle in Heidelberg is very similar to the filtered modeled source signature in amplitude as well as in phase (blue line in Fig. 4).

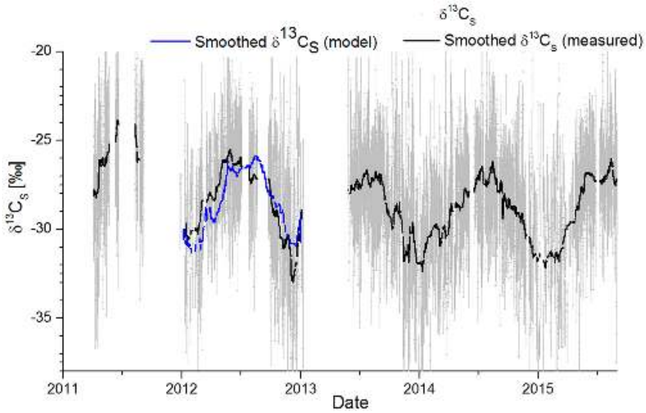

Figure 4. Moving Keeling plot method-based source signature in Heidelberg from 2011 until mid-2015. The black line is the smoothed measured source signature, and the blue line gives the smoothed modeled source signature (both 50th-percentile filter with window size = 100 h). Half a window size before the beginning of a large data gap the data are not further smoothed to prevent smoothing artifacts.

3.3 Information content derived from δ_S

We now want to elaborate what quantitative information can be drawn from the mean source signature record in Heidelberg about its components. For an urban continental measurement site, we have to assume that there are at least two main source types of CO_2 in the catchment area: fuel CO_2 and CO_2 from the biosphere. In this simplest case, we essentially have one equation for δ_S (Eq. 6) with three unknown variables (δ_{bio}, δ_F and the fuel (or biosphere) share f_F); only if two of these variables are known can the third variable be quantified from the measurements:

$$\delta_S = \frac{CO_{2F}}{\Delta CO_2} \cdot \delta_F + \frac{\Delta CO_2 - CO_{2F}}{\Delta CO_2} \cdot \delta_{bio} \quad (5)$$

$$= f_F \cdot \delta_F + (1 - f_F) \cdot \delta_{bio}. \quad (6)$$

Which of the variables is the one to be estimated depends, of course, on the research question. If the fossil fuel share and end members are well known from inventories, one could be especially interested in determining the isotopic end member δ_{bio} in order to study biospheric processes and their feedback to climatic parameters (Ciais et al., 2005; Ballantyne et al., 2010; Salmon et al., 2011). Contrarily, one may be interested in determining the relative share of fossil fuel CO_2 in the catchment area (with known δ_{bio} and δ_F) to monitor emission changes independently from emission inventories.

As noted, a quantification of the relative shares of fossil fuel and the biospheric CO_2 at continental stations is only possible if information on the isotopic end members of both source categories is available. For example, Vardag et al. (2015b) used the isotopic signatures of δ_{bio} (assumed to be known within a fixed uncertainty) and δ_F (obtained by calibration with $\Delta^{14}C(CO_2)$) to calculate the fossil fuel CO_2 contribution from the (continuously) measured CO_2 and $\delta^{13}C(CO_2)$ signal. However, knowing the isotopic signatures δ_{bio} and δ_F over the entire course of the year requires an extensive number of measurements at the relevant sources throughout the year and further assumptions of how to scale up these point measurements to a mean source signature of all relevant sources. Therefore, the question, which we address here, is whether it is possible to obtain information on these end members from our measured source signature record, despite the fact that we have three unknown variables and only one equation. In the following, we discuss this question exemplary for the year 2012, for which we have modeled data, inventory information and the mean measured isotope signature. We restrict the discussion to a single year as we focus on discussing which information can principally be obtained from a year-round mean source signature record.

We have noted that, in order to obtain information from δ_S on δ_{bio} (δ_F), we require information on the fuel CO_2 share and δ_F (on the fuel CO_2 share and δ_{bio}). However, in cases where the relative share of the biosphere (fossil fuels) is negligible, the isotopic signature of δ_F (δ_{bio}) would equal the mean measured isotopic signature. In these cases, the number of unknown variables would be reduced to one, as the fossil fuel (biospheric) share is $\approx 100\,\%$ and δ_{bio} (δ_F) does not contribute to the mean source signature. In a typical catchment area, the relative share of fossil fuels and of the biosphere will not be negligible throughout the year; however in winter, fossil fuel CO_2 will dominate, while in summer the biospheric CO_2 will dominate the CO_2 offset compared to the background. For example, from the STILT model results for Heidelberg (Sect. 3.1 and Appendix A), we perceive that on cold winter days in Heidelberg the fossil fuel share can be about 90 to 95 % of the total CO_2 offset. In summer, it reaches a minimum of about 20 %. We may, thus, be able to obtain information about the isotopic end members of δ_F in winter (δ_{bio} in summer), when the mean source signature is dominated by the fossil fuel (biospheric) share.

3.4 Evaluation of δ_S in Heidelberg

To calculate the isotopic end members of δ_i from the measured source signature in Heidelberg (and with that to solve Eq. 6), we require the fossil fuel CO_2 share, which we take here from STILT and the bottom-up emission inventory Emissions Database for Global Atmospheric Research (EDGARv4.3; EC-JCR/PBL, 2015). However, as we only require the share and not the absolute concentration, we are largely independent from potentially large model transport errors. We thus assume an absolute uncertainty of 10 % of the fossil fuel share (and of the biospheric share).

To determine δ_F in addition to the fuel CO_2 share, we require a value for δ_{bio}. Here we use a typical mean value of the isotopic end member of $\delta_{bio} = -25.0\,‰$ and assume a seasonal cycle as determined for Europe by Ballantyne et al. (2011) (see Figs. 2 and 3 in Ballantyne et al., 2011) displayed in Fig. 5a as a solid green line. We show δ_{bio} with two possible uncertainties of 0.5 and 2.0 ‰. As expected, the uncertainty of the unknown δ_F is only acceptably small when the relative share of the biosphere becomes negligible, which is the case in winter (Fig. 5a). The isotopic end member of δ_F in winter is about (-31.0 ± 2.5) ‰ in January to March 2012 and decreases to (-32.5 ± 2.5) ‰ in November to December 2012. Further, Fig. 5a shows that the best estimate of the resulting isotopic signature δ_F is more depleted in summer than in winter. This curvature is the opposite of what we would expect from EDGAR transported by STILT (see assumed δ_F in Fig. 5b). Only when assuming an uncertainty of the biospheric end member of $\pm 2\,‰$ or more, the uncertainty range of the estimated δ_F allows a more enriched δ_F signature in summer than in winter. This suggests that the isotopic source signature of the biosphere in summer is most probably more depleted (by about 2 ‰) than the previously assumed δ_{bio} value based on Ballantyne et al. (2011).

To estimate δ_{bio} (Fig. 5b), we require (besides the fossil fuel share) the isotopic source signature δ_F. Here we use δ_F calculated with the STILT model on the basis of EDGAR emissions and source signatures according to Table A1. Its annual mean value is $-31.0\,‰$, and it shows a seasonal cycle with more enriched signatures in summer than in winter. We show the results for δ_{bio} for two possible δ_F uncertainties of 1.0 and 3.0 ‰ (see Fig. 5b). The best estimate of the isotopic end member of δ_{bio} in summer is about $-25.0 \pm 1.0\,‰$ in June to August 2012. This reinforces the presumption that δ_{bio} is more depleted than the assumed δ_{bio} value based on Ballantyne et al. (2011) during summer.

The uncertainty of the isotopic end members in Fig. 5a and b has three components: (1) the uncertainty of the fossil fuel CO_2 share estimated from STILT, which we assume to be about 10 % (absolute) in our case; (2) the uncertainty of the other known isotopic end member (0.5 and 2 ‰ for δ_{bio} or 1.0 and 3.0 ‰ for δ_F); and (3) the uncertainty of the measured mean source signature itself (ca. 0.4 ‰; see Sect. 3.1 for interquartile range of difference between smoothed regression-based and smoothed modeled source signature). Note that an uncertainty of 10 % of the fossil fuel share is at the low end of uncertainties. However, an uncertainty of 20 % of the fossil fuel share would increase the uncertainty in the unknown isotopic end members by only 0.2–0.4 ‰ for δ_{bio} in summer and δ_F in winter.

The derived uncertainty of δ_F is about 2.5 ‰ in winter, and that of δ_{bio} is about 1.0 ‰ in summer. An uncertainty of $\pm 2.5\,‰$ for δ_F is rather large if we want to use this observation-based top-down result for further quantitative source apportionment. Vardag et al. (2015b) showed that a misassignment of 2.5 ‰ in δ_F leads to a bias in the continuous fuel CO_2 estimate of about 15 % for an urban measurement site like Heidelberg. The observation-based biospheric end member δ_{bio} has an uncertainty of only about 1.0 ‰ in

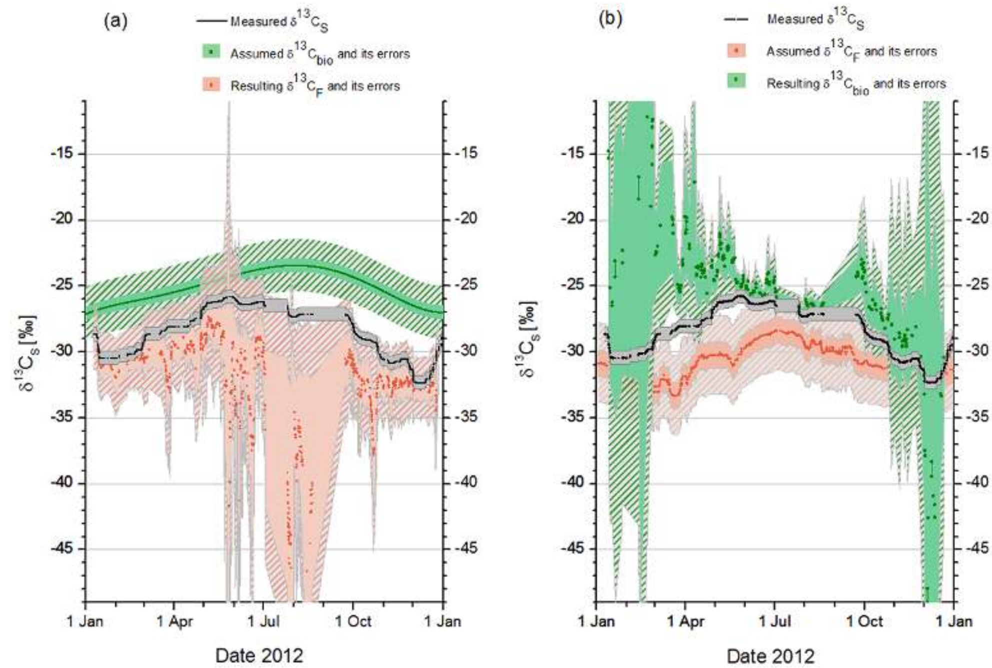

Figure 5. (a) A fixed isotopic end member of the biosphere (green, ±uncertainty of 0.5 ‰ (light green area) and 2 ‰ (crosshatched green)) together with the measured source signature (black) results in δ_F (red, ±its uncertainty). **(b)** A fixed isotopic end member of the fuel mix (red, ±uncertainty of 1.0 ‰ (salmon pink) and 2.0 ‰ (crosshatched gray-pink)) together with the measured source signature (black) results in δ_{bio} (green, ±its uncertainty). In both cases, also the fuel CO_2 share (or biospheric CO_2 share) is required. We here use the share calculated with STILT on the basis of EDGAR v4.3 and assume an absolute uncertainty of 10 %.

June to August 2012, which is a very well constrained value for this period.

We cannot assume that the isotopic end members δ_{bio} and δ_F remain constant over the course of the year: δ_{bio} typically shows a seasonal cycle possibly due to seasonal changes in the fraction of respiration from C3/C4 plants as well as due to influences of meteorological conditions on biospheric respiration. Likewise, δ_F typically shows more enriched values in summer, when the contribution of residential heating (and therewith of depleted natural gas) is much smaller than in winter. Therefore, no year-round estimation of fuel CO_2 share is possible from only CO_2 and $\delta^{13}C(CO_2)$ either.

4 Summary and conclusions

Many measurement stations are currently being equipped with new optical instruments which measure $\delta^{13}C(CO_2)$, aiming at an improved quantitative understanding of the carbon fluxes in their catchment area. If this additional $\delta^{13}C(CO_2)$ data stream is not directly digested in regional model calculations, the mean isotopic source signature is often computed from the $\delta^{13}C(CO_2)$ and CO_2 records for a potential partitioning of source contributions. A bias-free determination of source signature, however, requires carefully selecting the data for situations in which determination of source signature with a Keeling plot method can provide reliable results. This excludes periods (1) when sinks and sources occur simultaneously, (2) when the source mix changes or (3) when the signal-to-noise ratio is too low (Keeling, 1958; 1961; Miller and Tans, 2003).

We therefore developed filter criteria and show that the routine and accurate determination of $\delta^{13}C(CO_2)$ source signature is possible if the introduced filter criteria are applied. As suggested by Röckmann et al. (2016), we use a modeled dataset for validation of the approach. We find that for a station like Heidelberg the bias introduced by our analysis is only (0.2 ± 1.2) ‰ for hourly data. The uncertainty decreases in the long-term to (0.0 ± 0.4) ‰. We are, therefore, able to estimate the source signature correctly, but 85 % of the data are rejected by the filter criteria. Further, as the filter criteria are such that the source signatures are more likely to be filtered out during the day than during the night, the long-term source signature is not representative of real daily averages, but only of periods where the data were not filtered out (mainly nighttime). As a consequence, the isotopic end members δ_{bio} and δ_F can also only be estimated for these periods. This problem does not occur for CH_4, which has only weak daytime sinks.

By applying the moving Keeling plot method to a real dataset measured in Heidelberg, we were able to determine the source signature over the course of 4 years. We find a distinct seasonal cycle of the mean source signature with values of about −26 ‰ in summer and about −32 ‰ in winter. This general behavior was expected due to the larger relative contribution of more depleted fossil fuel CO_2 in winter. For a unique interpretation of the mean source signature, possible sources in the catchment area need to be identified. As soon as there is more than one source, the source signature is a function of the isotopic end members of all sources, as well as of their relative shares. Therefore, to study the seasonal and diurnal changes of fossil fuel shares at a continental station, information on the isotopic end members of the fossil fuel mix as well as of the biosphere is required at the same time resolution. Unfortunately, the isotopic end members are often not known with high accuracy. The uncertainty of the isotopic end members often impedes or even prevents a unique straightforward determination of the source contribution in the catchment area (e.g., Pataki, 2003; Torn et al., 2011, Lopez et al. 2013; Röckmann et al., 2016) and calls for elaborated statistical models based on Bayesian statistics. This important fact is sometimes mentioned, but the consequences for quantitative evaluations are rarely emphasized, preserving the high expectations associated with isotope measurements.

We showed that for the urban site of Heidelberg we can use the observation-based mean source signature record to estimate the isotopic end member δ_F in winter and the isotopic end member δ_{bio} in summer within the uncertainties of ±2.5 and ±1.0 ‰, respectively. Here we assumed an uncertainty of ±10 % for the fossil fuel and the biospheric CO_2 share and an uncertainty of the other isotopic end member δ_F of ±3.0 ‰ and δ_{bio} of ±2.0 ‰. However, in the winter season we cannot obtain any reliable information on δ_{bio}, and in summer we cannot study δ_F. For a year-round determination of fossil fuel share, δ_{bio} and δ_F are required throughout the year. As no reliable determination of δ_{bio} and δ_F is possible during the entire year based only on atmospheric observations, there is a need for either very good bottom-up information for the catchment area of interest or frequent measurement campaigns close to the sources. However, the disadvantage of using such a bottom-up approach is that usually only information from a few specific sites are available, which need then to be upscaled correctly such that they are representative of the entire catchment area. For a determination of δ_F during the entire year, one can possibly utilize $\Delta^{14}C(CO_2)$ and CO/CO_2 measurements (following Vardag et al. (2015b)) or O_2/N_2 measurements (e.g., Sturm et al. 2006; Steinbach et al., 2011), all of which exhibit their own deficiencies, which are discussed elsewhere (e.g., Ciais et al., 2015; Vardag et al., 2015b).

Finally, we could show that, even though it is not possible to determine the isotopic end members throughout the year, it is possible to refute certain literature values. For example, a respiration signature of −23 ‰ in August and September 2012 as reported by Ballantyne et al. (2011) is most likely too enriched as this would lead to more depleted δ_F values in summer than in winter. This is in contrast to what we would expect based on emission inventories.

5 Data availability

The CO_2 and $\delta^{13}C(CO_2)$ records from the measurement site Heidelberg are available at http://www.iup.uni-heidelberg.de/institut/forschung/groups/kk/Data/Hourly_FTIR.txt.
In future, this dataset will also be accessible via the ICOS Carbon portal. CO_2 flask data from Mace Head (Dlugokencky et al., 2015) can be downloaded at ftp://aftp.cmdl.noaa.gov/data/trace_gases/co2/flask/surface/. The $\delta^{13}C(CO_2)$ flask data from Mace Head (White et al., 2015) can be downloaded at ftp://aftp.cmdl.noaa.gov/data/trace_gases/co2c13/flask/ftp://aftp.cmdl.noaa.gov/data/trace_gases/co2c13/flask/. The emission inventory data from EDGAR is available at http://edgar.jrc.ec.europa.eu/index.php. The BP Statistical Review of World Energy for the year 2015 is avaliable at http://www.bp.com/en/global/corporate/energy-economics/statistical-review-of-world-energy/2015-in-review.html.

Appendix A: The STILT model

We use the STILT model (Lin et al., 2003) to evaluate our moving Keeling plot method. The STILT model computes the CO_2 mole fraction by time-inverting meteorological fields and tracing particles emitted at the measurement location back in time to identify where the air parcel originated from. This so-called footprint area is then multiplied by the surface emissions in the footprint to obtain the CO_2 concentration at the site in question. Photosynthesis and respiration CO_2 fluxes are taken from the vegetation photosynthesis and respiration model (VPRM, Mahadevan et al., 2008). Anthropogenic emissions are taken from EDGAR v4.3 emission inventory (EC-JRC/PBL, 2015) for the base year 2010 and further extrapolated to the year 2012 using the BP Statistical Review of World Energy 2015 (available at http://www.bp.com/en/global/corporate/energy-economics/statistical-review-of-world-energy/2015-in-review.html).
Additionally, we use seasonal, weekly and daily time factors for different emission categories (Denier van der Gon et al., 2011). Since the EDGAR inventory is separated into different fuel types, we obtain a CO_2 record for each fuel type as well as for respiration and photosynthesis. This allows us to construct a corresponding $\delta^{13}C(CO_2)$ record by multiplying the isotopic signature of every emission group i to its respective CO_2 mole fraction $\delta^{13}C(CO_2)_i \cdot CO_{2,i}$ (see Table A1), adding these to a far-field boundary value of $\delta^{13}C(CO_2) \times CO_2$ and dividing it by the total CO_2 at the model site. The CO_2 far-field boundary value for STILT is the concentration at the European domain border (16° W to 36° E and from 32 to 74° N) at the position where the backwards-traced particles leave the domain. The concentration at the domain border is taken from analyzed CO_2 fields generated with TM3 (Heimann and Körner, 2003) based on optimized fluxes (Rödenbeck, 2005). The isotopic boundary value is then constructed artificially by fitting the linear regression between CO_2 and $\delta^{13}C(CO_2)$ in Mace Head (year 2011 from World Data Center for Greenhouse Gases; Dlugokencky et al. (2015)) and applying the function of the regression to the boundary CO_2 values in the model. Since, in reality, we also have measurement uncertainties of CO_2 and $\delta^{13}C(CO_2)$, we also include a random measurement uncertainty of 0.05 ppm and 0.05 ‰, respectively, to the modeled datasets. The CO_2 and $\delta^{13}C(CO_2)$ records are used to calculate the regression-based mean source signature following the moving Keeling plot method (Sect. 2.2).

A1 Computation of mean modeled source signature

For the reference modeled mean source signature we use a "moving" background. In particular, we chose the minimum CO_2 value within 5 h centered around the measurement point as the background value and all contributions from fuel CO_2 ($c_{F,i}$), respiration (c_{resp}) and photosynthesis (c_{photo}) are computed as offsets relative to the background (c_{bg}). This is then comparable to the regression-based moving Keeling plot method as the lowest and highest CO_2 values within 5 h span the Keeling plot. We are then able to define and compute the reference modeled mean source signature as

$$\delta_{\mathrm{S}}^{\mathrm{STILT}} = \frac{\sum_i \delta_{F,i}|c_{F,i}| + \delta_{\mathrm{resp}}|c_{\mathrm{resp}}| + \delta_{\mathrm{photo}}|c_{\mathrm{photo}}|}{\sum_i |c_{F,i}| + |c_{\mathrm{resp}}| + |c_{\mathrm{photo}}|}. \qquad \text{(A1)}$$

Note that we use absolute values of all contributions since photosynthetic contributions (c_{photo}) are generally negative while source contributions (c_{resp} and $c_{F,i}$) are generally positive, but both should lead to a negative source signature in a Keeling plot. The calculated source signature $\delta_{\mathrm{S}}^{\mathrm{STILT}}$ (from Eq. A1) can be seen in Fig. 2a (blue). If we did not take into account the different signs of respiration and photosynthesis, we would construct isotopic signatures which are counterintuitive and not interpretable as the mean source signature (Miller and Tans, 2003) as the denominator could converge against zero. When calculating the isotopic source following Eq. (A1), we can interpret $\delta_{\mathrm{S}}^{\mathrm{STILT}}$ as gross flux-weighted mean isotopic signature of sources and sinks.

Table A1. $\delta^{13}C(CO_2)$ source signature of fuel types and biosphere as used in the model and the range of literature values. Note that for a specified region the range of possible isotopic signature can often be narrowed down if the origin and/or production process of the fuel type is known.

Emission source	Used $\delta_{F,i}$ or δ_{bio} [‰]	Range of literature values $\delta_{F,i}$ or δ_{bio} [‰]	Reference
Fuel types			
Coal		−23 to −27	Mook (2000)
– Hard coal	−25		
– Brown coal	−27		
Peat	−28	−22 to −29	Mook (2000); Schumacher et al. (2011)
Oil	−29	−19 to −35	Andres et al. (1994); Mook (2000); Schumacher et al. (2011)
Gas			
– Natural gas	−46	−20 to −100	Andres et al. (1994)
– Derived gas	−28	−26 to −29	Bush et al. (2007)
Solid waste	−28	−20 to −30	Typical range of C3 and C4 plant mixes (Mook, 2000)
Solid biomass	−27	−20 to −30	Typical range of C3 and C4 plant mixes (Mook, 2000)
Bio liquid	−29	−20 to −30	Typical range of C3 and C4 plant mixes (Mook, 2000)
Biogas	−11	0 to −16	Levin et al. (1993; Widory et al. (2012))
Biosphere		−20 to −30	Lloyd and Farquhar (1994); Mook (2000)
Photosynthesis	−23	−20 to −30	Typical range of C3 and C4 plant mixes (Mook, 2000)
Respiration	−25	−20 to −30	Typical range of C3 and C4 plant mixes (Mook, 2000)

Appendix B: CO_2 and $\delta^{13}C(CO_2)$ measurements in Heidelberg

A necessary prerequisite of determining the mean source signature correctly at a measurement site is a good quality of CO_2 and $\delta^{13}C(CO_2)$ measurements. Therefore, we briefly describe here the instrumental setup in Heidelberg, assess the precision of the CO_2 and $\delta^{13}C(CO_2)$ measurements and finally present our 4-year ambient air record of CO_2 and $\delta^{13}C(CO_2)$ in Heidelberg.

B1 Instrumental setup and intermediate measurement precision

Since April 2011, atmospheric trace gas mole fractions are measured with an in situ Fourier transform infrared (FTIR) spectrometer at 3 min time resolution at the Institut für Umweltphysik in Heidelberg (Germany, 49°25′ N, 8°41′ E, 116 m a.s.l +30 m a.g.l.) (see Fig. B1 for CO_2 and $\delta^{13}C(CO_2)$). A description of the measurement principle can be found in Esler et al. (2000) and Griffith et al. (2010, 2012). Hammer et al. (2013) describe the Heidelberg-specific instrumental setup in detail, and Vardag et al. (2015a) describe modifications to this setup and the calibration strategy for the stable isotopologue measurements. The dataset is available at http://www.iup.uni-heidelberg.de/institut/forschung/groups/kk/Data/Hourly_FTIR.txt.

The intermediate measurement precision of the FTIR is about 0.05 ppm for CO_2 and 0.04 ‰ for $\delta^{13}C(CO_2)$ (both 9 min averages) as determined from the variation of daily target gas measurements (Vardag et al., 2014; Vardag et al., 2015a). In this work, we only use hourly CO_2 and $\delta^{13}C(CO_2)$ values, since simulation runs often have an hourly resolution, and thus observations and simulations can directly be compared. However, from Allan standard deviation tests, we know that the intermediate measurement precision of hourly measurements is only slightly better than for 9-minutely measurements (Vardag et al., 2015a).

B2 Four years of concurrent CO_2 and $\delta^{13}C(CO_2)$ measurements in Heidelberg

The CO_2 concentration in Heidelberg varies over the course of the year and has its maximum in winter and its minimum in summer (Fig. B1). This pattern is mainly driven by larger fossil fuel emissions in winter than in summer. In particular, emissions from residential heating are higher in the cold season. Furthermore, biospheric uptake of CO_2 is lower in winter than in summer. The minimum of the isotopic $\delta^{13}C(CO_2)$ value coincides with the maximum in CO_2 concentration and vice versa. The features are anticorrelated since almost all CO_2 sources in the catchment area of Heidelberg are more δ^{13}C-depleted than the background concentration, and therefore a CO_2 increase always leads to a depletion of $\delta^{13}C(CO_2)$ in atmospheric CO_2. In addition, the biospheric CO_2 sink, dominating in summer, discriminates against $\delta^{13}C(CO_2)$, leaving the atmosphere enriched in $^{13}C(CO_2)$, while CO_2 decreases. On top of the seasonal cycle, CO_2 in Heidelberg (Fig. B1) slightly increases over the course of 4 years by about 2 ppm yr^{-1}. At the same time $\delta^{13}C(CO_2)$ decreases by about 0.04 ‰ yr^{-1}. These rates are similar to the CO_2 increase and $\delta^{13}C(CO_2)$ decrease rates in Mauna Loa, Hawaii, USA (Dlugokencky et al., 2015; White et al., 2015), and therefore reflect the global increase of CO_2 from ^{13}C-depleted sources moderated by air–sea gas exchange. It is not visible to the eye how the degree of depletion in $\delta^{13}C(CO_2)$ varies over the course of the year (see Fig. B1). To analyze this behavior, the mean source signature must be computed (see Sect. 2.2 and Fig. 4).

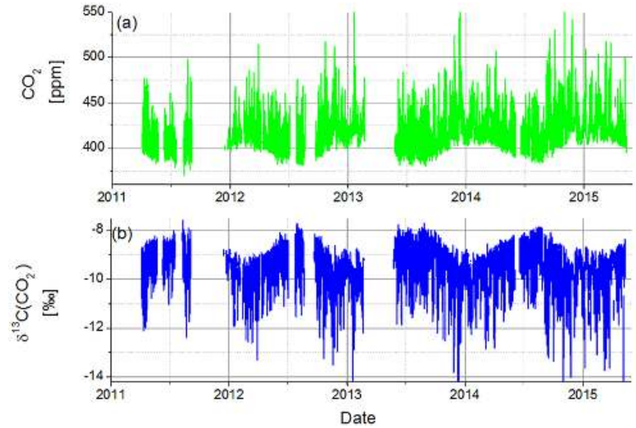

Figure B1. Continuous Heidelberg hourly FTIR record of **(a)** CO_2 and **(b)** $\delta^{13}C(CO_2)$ from April 2011 to June 2015. Data gaps occur when the instrument was away during a measurement campaign or when instrumental problems occurred.

Author contributions. Sanam Noreen Vardag developed the moving Keeling plot method in conjunction with Ingeborg Levin. Sanam Noreen Vardag verified this approach using pseudo data from the STILT model and applied the approach to measured data. The measured data were partly taken by Samuel Hammer (until September 2011) and mainly by Sanam Noreen Vardag (September 2011 to June 2015). The final discussion and manuscript writing profited from input from all three authors.

Acknowledgements. This work has been funded by the InGOS EU project (284274) and national ICOS BMBF project (01LK1225A) funded by the German Ministry of Education and Research (contract number: 01LK1225A). We thank NOAA/ESRL and INSTAAR for making their observational data from Mace Head and Mauna Loa available on the WDCGG website. Further, we acknowledge the financial support given by Deutsche Forschungsgemeinschaft and Ruprecht-Karls-Universität Heidelberg within the funding program Open Access Publishing.

Edited by: F. Joos
Reviewed by: two anonymous referees

References

Alden, C. B., Miller, B., J., and White, J. W.: Can bottom-up ocean CO_2 fluxes be reconciled with atmospheric ^{13}C observations?, Tellus B, 62, 369–388, doi:10.1111/j.1600-0889.2010.00481.x, 2010.

Andres, R. J., Marland, G., Boden, T., and Bischof, S.: Carbon Dioxide Emissions from Fossil Fuel Consumption and Cement Manufacture, 1751–1991; and an Estimate of Their Isotopic Composition and Latitudinal Distribution, Environmental Sciences, http://www.osti.gov/scitech/biblio/10185357 (last access: 22 July 2016), 1994.

Ballantyne, A. P., Miller, J. B., and Tans, P. P.: Apparent seasonal cycle in isotopic discrimination of carbon in the atmosphere and biosphere due to vapor pressure deficit, Global Biogeochem. Cy., 24, gB3018, doi:10.1029/2009GB003623, 2010.

Ballantyne, A. P., Miller, J. B., Baker, I. T., Tans, P. P., and White, J. W. C.: Novel applications of carbon isotopes in atmospheric CO_2: what can atmospheric measurements teach us about processes in the biosphere?, Biogeosciences, 8, 3093–3106, doi:10.5194/bg-8-3093-2011, 2011.

Bastos, A., Janssens, I. A., Gouveia, C. M., Trigo, R. M., Ciais, P., Chevallier, F., Peñuelas, J., Rödenbeck, C., Piao, S., Friedlingstein, P., and Running, S. W.: European land CO_2 sink influenced by NAO and East-Atlantic Pattern coupling, Nature Communications, 7, 10315, doi:10.1038/ncomms10315, 2016.

Bowling, D. R., Sargent, S. D., Tanner, B. D., and Ehleringer, J. R.: Tunable diode laser absorption spectroscopy for stable isotope studies of ecosystem-atmosphere CO_2 exchange, Agr. Forest Meteorol., 118, 1–19, doi:10.1016/S0168-1923(03)00074-1, 2003.

Bush, S., Pataki, D., and Ehleringer, J.: Sources of variation in $\delta^{13}C$ of fossil fuel emissions in Salt Lake City, USA, Appl. Geochem., 22, 715–723, 2007.

Ciais, P., Tans, P. P., Trolier, M., White, J. W. C., and Francey, R.: A large Northern Hemisphere terrestrial CO_2 sink indicated by the ^{13}C / ^{12}C ratio of atmospheric CO_2, Science, 269, 1098–1102, 1995.

Ciais, P., Reichstein, M., Viovy, N., Granier, A., Ogee, J., Allard, V., Aubinet, M., Buchmann, N., Bernhofer, C., Carrara, A., Chevalier, F., De Noblet, N., Friend, A. D., Friedlingstein, P., Grunwald, T., Heinesch, B., Keronen, P., Knohl, A., Krinner, G., Loustau, D., Manca, G., Matteucci, G., Miglietta, F., Ourcival, J. M., Papale, D., Pilegaard, K., Rambal, S., Seufert, G., Soussana, J. F., Sanz, M. J., Schulze, E. D., Vesala, T., and Valentini, R.: Europe-wide reduction in primary productivity caused by the heat and drought in 2003, Nature, 437, 529–533, 2005.

Ciais, P., Crisp, D., Denier van der Gon, H., Engelen, R., Janssens-Maenhout, G., Heiman, M., Rayner, P., and Scholze, M.: Towards a European Operational Observing System to Monitor Fossil CO_2 Emissions, Study report, Tech. rep., Copernicus, http://www.copernicus.eu/main/towards-european-operational-observing-system-monitor (last access: 4 July 2016), 2015.

Denier van der Gon, H., Hendriks, C., Kuenen, J., Segers, A., and Visschedijk, A.: Description of current temporal emission patterns and sensitivity of predicted AQ for temporal emission patterns, TNP Report, EU FP7 MACC deliverable report, https://gmes-atmosphere.eu/documents/deliverables/d-emis/MACC_TNO_del_1_3_v2.pdf (last access: 22 July 2016), 2011.

Dlugokencky, E., Lang, P., Masarie, K., Crotwell, A., and Crotwell, M.: Atmospheric Carbon Dioxide Dry Air Mole Fractions from the NOAA ESRL Carbon Cycle Cooperative Global Air Sampling Network Sampling Network, 1968–2014, ftp://aftp.cmdl.noaa.gov/data/trace_gases/co2/flask/surface/ (last access: 4 July 2016), 2015.

EC-JRC/PBL: Emission Database for Global Atmospheric Research (EDGAR), version 4.3., http://edgar.jrc.ec.europa.eu/index.php, last access: 10 December 2015.

Esler, M. B., Griffith, D. W., Wilson, S. R., and Steele, L. P.: Precision trace gas analysis by FT-IR spectroscopy. 2. The ^{13}C / ^{12}C isotope ratio of CO_2, Anal. Chem., 72, 216–21, 2000.

Eyer, S., Tuzson, B., Popa, M. E., van der Veen, C., Röckmann, T., Rothe, M., Brand, W. A., Fisher, R., Lowry, D., Nisbet, E. G., Brennwald, M. S., Harris, E., Zellweger, C., Emmenegger, L., Fischer, H., and Mohn, J.: Real-time analysis of $\delta^{13}C$- and δD-CH_4 in ambient air with laser spectroscopy: method development and first intercomparison results, Atmos. Meas. Tech., 9, 263–280, doi:10.5194/amt-9-263-2016, 2016.

Griffith, D., Deutscher, N., Krummel, P., Fraser, P., Schoot, M., and Allison, C.: The UoW FTIR trace gas analyser: Comparison with LoFlo, AGAGE and tank measurements at Cape Grim and GASLAB, Baseline atmospheric program (Australia), 2010.

Griffith, D. W. T., Deutscher, N. M., Caldow, C., Kettlewell, G., Riggenbach, M., and Hammer, S.: A Fourier transform infrared trace gas and isotope analyser for atmospheric applications, Atmos. Meas. Tech., 5, 2481–2498, doi:10.5194/amt-5-2481-2012, 2012.

Gurney, K. R., Mendoza, D. L., Zhou, Y., Fischer, M. L., Miller, C. C., Geethakumar, S., and de la Rue du Can, S.: High resolution fossil fuel combustion CO_2 emission fluxes for the United States, Environ. Sci. Technol., 43, 5535–5541, 2009.

Hammer, S., Griffith, D. W. T., Konrad, G., Vardag, S., Caldow, C., and Levin, I.: Assessment of a multi-species in situ FTIR for precise atmospheric greenhouse gas observations, Atmos. Meas. Tech., 6, 1153–1170, doi:10.5194/amt-6-1153-2013, 2013.

Heimann, M. and Körner, S.: The global atmospheric tracer model TM3, in: Technical Report, edited by: Biogeochemie, edited by: Körner, S., vol. 5, p. 131, Max-Planck-Institut für Biogeochemie, Jena, 2003.

Karlsson, J., Jansson, M., and Jonsson, A.: Respiration of allochthonous organic carbon in unproductive forest lakes determined by the Keeling plot method, Limnol. Oceanogr., 52, 603–608, doi:10.4319/lo.2007.52.2.0603, 2007.

Keeling, C. D.: The concentration and isotopic abundances of atmospheric carbon dioxide in rural areas, Geochim. Cosmochim. Ac., 13, 322–224, 1958.

Keeling, C. D.: The concentrations and isotopic abundances of atmospheric carbon dioxide in rural and marine air, Geochim. Cosmochim. Ac., 24, 277–298, 1961.

Knohl, A., Werner, R. A., Brand, W. A., and Buchmann, N.: Short-term variations in $\delta^{13}C$ of ecosystem respiration reveals link between assimilation and respiration in a deciduous forest, Oecologia, 142, 70–82, doi:10.1007/s00442-004-1702-4, 2005.

Krystek, M. and Anton, M.: A weighted total least-squares algorithm for fitting a straight line, Meas. Sci. Technol., 18, 3438, doi:10.1088/0957-0233/18/11/025, 2007.

Lai, C.-T., Ehleringer, J. R., Tans, P., Wofsy, S. C., Urbanski, S. P., and Hollinger, D. Y.: Estimating photosynthetic ^{13}C discrimination in terrestrial CO_2 exchange from canopy to regional scales, Global Biogeochem. Cy., 18, gB1041, doi:10.1029/2003GB002148, 2004.

Levin, I., Bergamaschi, P., Dörr, H., and Trapp, D.: Stable isotopic signature of methane from major sources in Germany, Chemosphere, proceedings of the NATO advanced research workshop, 26, 161–177, doi:10.1016/0045-6535(93)90419-6, 1993.

Lin, J., Gerbig, C., Wofsy, S. C., Andrews, A. E., Daube, B. C., Davis, K. J., and Grainger, C. A.: A near-field tool for simulating the upstream influence of atmospheric observations: The Stochastic Time-Inverted Lagrangian Transport (STILT) model, J. Geophys. Res., 108, 17 pp., doi:10.1029/2002JD003161, 2003.

Lloyd, J. and Farquhar, G. D.: ^{13}C discrimination during CO_2 assimilation by the terrestrial biosphere, Oecologia, 99, 201–215, 1994.

Lopez, M., Schmidt, M., Delmotte, M., Colomb, A., Gros, V., Janssen, C., Lehman, S. J., Mondelain, D., Perrussel, O., Ramonet, M., Xueref-Remy, I., and Bousquet, P.: CO, NO_x and $^{13}CO_2$ as tracers for fossil fuel CO_2: results from a pilot study in Paris during winter 2010, Atmos. Chem. Phys., 13, 7343–7358, doi:10.5194/acp-13-7343-2013, 2013.

Mahadevan, P., Wofsy, S. C., Matross, D. M., Xiao, X., Dunn, A. L., Lin, J. C., Gerbig, C., Munger, J. W., Chow, V. Y., and Gottlieb, E. W.: A satellite-based biosphere parameterization for net ecosystem CO_2 exchange: Vegetation Photosynthesis and Respiration Model (VPRM), Global Biogeochem. Cy., 22, doi:10.1029/2006GB002735, 2008.

Marland, G., Pielke Sr., R. A., Apps, M., Avissar, R., Betts, R. A., Davis, K. J., Frumhoff, P. C., Jackson, S. T., Joyce, L. A., Kauppi, P., Katzenberger, J., MacDicken, K. G., Neilson, R. P., Niles, J. O., Niyogi, D. S., Norby, R. J., Pena, N., Sampson, N., and Xue, Y.: The climatic impacts of land surface change and carbon management, and the implications for climate-change mitigation policy, Clim. Policy, 3, 149–157, doi:10.3763/cpol.2003.0318, 2003.

McManus, J. B., Nelson, D. D., and Zahniser, M. S.: Long-term continuous sampling of $^{12}CO_2$, $^{13}CO_2$ and $^{12}C^{18}O^{16}O$ in ambient air with a quantum cascade laser spectrometer, Isot. Environ. Healt. S., 46, 49–63, doi:10.1080/10256011003661326, 2010.

Miller, J. B. and Tans, P. P.: Calculating isotopic fractionation from atmospheric measurements at various scales, Tellus, 55, 207–214, 2003.

Mook, W. G.: Environmental isotopes in the hydrological cycle – Principles and applications, Technical Documents in Hydrology, I, 2000.

Mook, W. G., Koopmans, M., Carter, A. F., and Keeling, C. D.: Seasonal, latitudinal, and secular variations in the abundance and isotopic ratios of atmospheric carbon dioxide: 1. Results from land stations, J. Geophys. Res., 88, 10915–10933, doi:10.1029/JC088iC15p10915, 1983.

Moore, J. and Jacobson, A. D.: Seasonally varying contributions to urban CO_2 in the Chicago, Illinois, USA region: Insights from a high-resolution CO_2 concentration and $\delta^{13}C$ record, Elementa: Science of the Anthropocene, 3, 000052, doi:10.12952/journal.elementa.000052, 2015.

Newman, S., Xu, X., Gurney, K. R., Hsu, Y. K., Li, K. F., Jiang, X., Keeling, R., Feng, S., O'Keefe, D., Patarasuk, R., Wong, K. W., Rao, P., Fischer, M. L., and Yung, Y. L.: Toward consistency between trends in bottom-up CO_2 emissions and top-down atmospheric measurements in the Los Angeles megacity, Atmos. Chem. Phys., 16, 3843-3863, doi:10.5194/acp-16-3843-2016, 2016.

Ogée, J., Peylin, P., Cuntz, M., Bariac, T., Brunet, Y., Berbigier, P., Richard, P., and Ciais, P.: Partitioning net ecosystem carbon exchange into net assimilation and respiration with canopy-scale isotopic measurements: An error propagation analysis with $^{13}CO_2$ and $CO^{18}O$ data, Global Biogeochem. Cy., 18, gB2019, doi:10.1029/2003GB002166, 2004.

Pataki, D. E.: The application and interpretation of Keeling plots in terrestrial carbon cycle research, Global Biogeochem. Cy., 17, 1022, doi:10.1029/2001GB001850, 2003.

Röckmann, T., Eyer, S., van der Veen, C., Popa, M. E., Tuzson, B., Monteil, G., Houweling, S., Harris, E., Brunner, D., Fischer, H., Zazzeri, G., Lowry, D., Nisbet, E. G., Brand, W. A., Necki, J. M., Emmenegger, L., and Mohn, J.: In-situ observations of the isotopic composition of methane at the Cabauw tall tower site, Atmos. Chem. Phys. Discuss., doi:10.5194/acp-2016-60, in review, 2016.

Rödenbeck, C.: Estimating CO_2 sources and sinks from atmospheric mixing ratio measurements using a global inversion of atmospheric transport, http://www.bgc-jena.mpg.de/bgc-systems/pmwiki2/uploads/Publications/6.pdf (last access: 21 July 2016), 2005.

Salmon, Y., Buchmann, N., and Barnard, R. L.: Response of $\delta^{13}C$ in plant and soil respiration to a water pulse, Biogeosciences Discuss., 8, 4493–4527, doi:10.5194/bgd-8-4493-2011, 2011.

Schmidt, M.: Messung und Bilanzierung anthropogener Treibhausgase in Deutschland, Dissertation, Universität Heidelberg, Heidelberg, 1999.

Schumacher, M., Werner, R. A., Meijer, H. A. J., Jansen, H. G., Brand, W. A., Geilmann, H., and Neubert, R. E. M.: Oxygen isotopic signature of CO_2 from combustion processes, Atmos. Chem. Phys., 11, 1473–1490, doi:10.5194/acp-11-1473-2011, 2011.

Steinbach, J., Gerbig, C., Rödenbeck, C., Karstens, U., Minejima, C., and Mukai, H.: The CO_2 release and Oxygen uptake from Fossil Fuel Emission Estimate (COFFEE) dataset: effects from varying oxidative ratios, Atmos. Chem. Phys., 11, 6855–6870, doi:10.5194/acp-11-6855-2011, 2011.

Sturm, P., Leuenberger, M., Valentino, F. L., Lehmann, B., and Ihly, B.: Measurements of CO_2, its stable isotopes, O_2/N_2, and ^{222}Rn at Bern, Switzerland, Atmos. Chem. Phys., 6, 1991–2004, doi:10.5194/acp-6-1991-2006, 2006.

Torn, M. S., Biraud, S. C., Still, C. J., Riley, W. J., and Berry, J. A.: Seasonal and interannual variability in ^{13}C composition of ecosystem carbon fluxes in the U.S. Southern Great Plains, Tellus B, 63, 181–195, doi:10.1111/j.1600-0889.2010.00519.x, 2011.

Tuzson, B., Zeeman, M., Zahniser, M., and Emmenegger, L.: Quantum cascade laser based spectrometer for in situ stable carbon dioxide isotope measurements, Infrared Physics and Technology, 51, 198–206, doi:10.1016/j.infrared.2007.05.006, 2008.

Vardag, S. N., Hammer, S., O'Doherty, S., Spain, T. G., Wastine, B., Jordan, A., and Levin, I.: Comparisons of continuous atmospheric CH_4, CO_2 and N_2O measurements – results from a travelling instrument campaign at Mace Head, Atmos. Chem. Phys., 14, 8403–8418, doi:10.5194/acp-14-8403-2014, 2014.

Vardag, S. N., Hammer, S., Sabasch, M., Griffith, D. W. T., and Levin, I.: First continuous measurements of $\delta^{18}O\text{-}CO_2$ in air with a Fourier transform infrared spectrometer, Atmos. Meas. Tech., 8, 579–592, doi:10.5194/amt-8-579-2015, 2015a.

Vardag, S. N., Gerbig, C., Janssens-Maenhout, G., and Levin, I.: Estimation of continuous anthropogenic CO_2: model-based evaluation of CO_2, CO, $\delta^{13}C(CO_2)$ and $\Delta^{14}C(CO_2)$ tracer methods, Atmos. Chem. Phys., 15, 12705–12729, doi:10.5194/acp-15-12705-2015, 2015b.

Vogel, F. R., Hammer, S., Steinhof, A., Kromer, B., and Levin, I.: Implication of weekly and diurnal ^{14}C calibration on hourly estimates of CO-based fossil fuel CO_2 at a moderately polluted site in southwestern Germany, Tellus B, 62, 512–520, doi:10.1111/j.1600-0889.2010.00477.x, 2010.

Vogel, F. R., Huang, L., Ernst, D., Giroux, L., Racki, S., and Worthy, D. E. J.: Evaluation of a cavity ring-down spectrometer for in situ observations of $^{13}CO_2$, Atmos. Meas. Tech., 6, 301–308, doi:10.5194/amt-6-301-2013, 2013.

White, J., Vaughn, B., and Michel, S.: Stable Isotopic Composition of Atmospheric Carbon Dioxide (^{13}C and ^{18}O) from the NOAA ESRL Carbon Cycle Cooperative Global Air Sampling Network, 1990–2014, ftp://aftp.cmdl.noaa.gov/data/trace_gases/co2c13/flask/ (last access: 16 March 2016), 2015.

Widory, D., Proust, E., Bellenfant, G., and Bour, O.: Assessing methane oxidation under landfill covers and its contribution to the above atmospheric CO_2 levels: The added value of the isotope ($\delta^{13}C$- and $\delta^{18}O\text{-}CO_2$; $\delta^{13}C$- and $\delta D\text{-}CH_4$) approach, Waste Manage., 32, 1685–1692, 2012.

Zobitz, J., Keener, J., Schnyder, H., and Bowling, D.: Sensitivity analysis and quantification of uncertainty for isotopic mixing relationships in carbon cycle research, Esevier-Agricultural and Forest Meteorology, 136, 2006.